THE ASTROPHYSICAL JOURNAL, 347:640–655, 1989 December 15

SMALL DENSE BROAD-LINE REGIONS IN ACTIVE NUCLEI

M. J. REES
Institute of Astronomy, Cambridge University

HAGAI NETZER
School of Physics and Astronomy and the Wise Observatory, Tel Aviv University, and Astronomy Department, Ohio State University

AND

G. J. FERLAND
Astronomy Department, Ohio State University
Received 1989 January 23; accepted 1989 June 17

ABSTRACT

Recent observational studies indicate that the broad-line region (BLR) of active galactic nuclei (AGN) may be much smaller than previously thought. One consequence is that the flux of ionizing radiation is considerably larger and the clouds may be denser than assumed in "standard photoionization models" for these objects. This paper attempts to investigate such questions by exploring realistic cloud distributions over a range of radii and densities. We propose some simple pressure laws and integrate over the radial distribution of clouds to obtain the contribution to the line and continuum emission for all parts of the BLR. This requires photoionization calculations at very high densities, up to 10^{13} cm^{-3}, and we discuss in detail the most important processes that are included and the improvements over previous calculations of this kind. In particular, hydrogen and helium are approximated as ~ 100 level systems, three-body recombination contribution to all elements is included, and we take full account of optical depth effects, including Stark broadening, in all lines. Finally, we predict line profiles, assuming that the cloud ensemble is in virial equilibrium.

The main results are as follows: (1) Most pressure laws imply a rapid increase of the covering factor with radius so that the emission-line spectrum of the ensemble is weighted toward the outside of the BLR. As a result, the gas distribution must be truncated at $N \sim 10^9$ cm^{-3} to prevent broad, strong O[III] lines. (2) Clouds of very high density are cooled mainly by free-free and recombination continua. The emergent spectrum of such clouds is very different from that observed in AGNs, having both strong ultraviolet lines, such as C III λ977, and Balmer and Paschen continuum. The fact that these are not observed sets a strong limit on the contribution of high-density material to the observed spectrum. (3) The observed C III] λ1909 line still provides the best indication that much of the gas is characterized by densities $N \sim 10^{10}$ cm^{-3}, but there is a nonnegligible contribution to the 1909 Å feature from Si III] λ1893. Si IV λ1397 is the dominant contribution to the 1400 Å blend at high densities. (4) Some models produce significant line emission from very small radii. However, these models can be ruled out because the predicted line profiles for different lines do not agree to the extent required by observations. Models which do produce similar line profiles tend to have their emissivity strongly weighted to either inner or outer radii, and it is difficult to force the ensemble to conspire to produce similar line profiles over a wide range of radii and density. (5) The best estimate of the BLR size, deduced from the new models, is smaller than in previous calculations, but it is still larger than indicated by some line reverberation measurements. Our normalization of the ionization parameter, based on old photoionization calculations, may thus be wrong.

Subject headings: galaxies: nuclei — quasars

I. INTRODUCTION

The earliest studies of quasar emission-line regions were concerned largely with establishing the basic ionization mechanism, the geometry, and the order-of-magnitude chemical composition (Bahcall and Koszlovsky 1969; Davidson 1972; MacAlpine 1972). For simplicity, and because the observations demanded no better, these studies considered the broad-line region to be characterized by a single value of the hydrogen density and "ionization parameter," the ratio of ionizing photon to hydrogen densities. They established that photoionization is the likely energy source, that the clouds producing the lines have coalesced into small filaments which are optically thick in the Lyman continuum, and that these clouds have, broadly speaking, a solar composition (see the review by Davidson and Netzer 1979). This kind of model for the broad-line region (BLR) is usually referred to as "the standard photoionization model."

Several serious limitations, especially those related to the hydrogen line problem (Baldwin 1977), precipitated several improvements to the photoionization models (see, for example, Weisheit, Shields, and Tarter 1979; Canfield and Puetter 1980; Kwan and Krolik 1981; Mushotzky and Ferland 1984; Kwan 1984; Netzer and Ferland 1984; Netzer, Elitzur, and Ferland 1985; Collin-Souffrin and Dumont 1986; Kallman and Krolik 1986). The main advances in the calculations were the improved treatment of hydrogen line transfer, along with X-ray related processes. Despite these studies, the hydrogen line problem is not yet solved, and there seem to be some other difficulties (e.g., the Fe II line problem; see Wills, Netzer, and Wills 1985) that were not realized before.

Recently, line reverberation studies of two or three low-luminosity AGNs (Peterson *et al.* 1985; Gaskell and Sparke 1986; Clavel, Wamsteker, and Glass 1987; Alloin *et al.* 1988) demonstrated yet another, perhaps even more severe, problem. The BLR size, inferred from the time lag between the continuum and line variations, is suspected to be 3–10 times smaller than is deduced from standard photoionization calculations. Large uncertainties are associated with the reverberation measurements, as well as with their interpretation (Peterson 1988; Edelson and Krolik 1988; Maoz and Netzer 1989), but it is almost certain that some fundamental model parameters will have to change in order to explain the new data. Also, a more realistic theory of the BLR must be developed; in particular, one which takes into account the fact that cloud parameters vary with position and that the BLR is actually three-dimensional.

The BLR size, deduced from photoionization calculations, is inversely proportional to the ionization parameter and the gas density, both of which are inferred from observations. The extension of current BLR models to encompass a more realistic situation, one in which the BLR is extended in distance, must, by necessity, consider clouds with densities much greater than those commonly assumed (i.e. $N \gg 10^{10}$ cm^{-3}). As a result, the microphysics which describes the equilibrium of the gas must be complete enough to include the approach to LTE, at least due to collisional processes at high densities. The extension of current theory to higher densities, and the distribution of gas at distances smaller than the classical $r_{\rm BLR}$, is the subject of this paer. In § II, we discuss the likely pressure and covering factor at $r < r_{\rm BLR}$. In § III we discuss in detail the physical processes needed to calculate the spectrum of dense gas, and § IV gives our new results and compares them with the observations. Finally, in § V, we discuss the application to AGN theory.

II. DISTRIBUTION OF BLR CLOUDS

We are interested in material distributed over a large range in radii, from very close to the continuum source, where the density is probably very large, to further out, at a radius where the density is more typical of previous calculations of this kind (the "standard BLR"). We consider a "cloud model" which is a concept adopted from the success of the standard photoionization model. We are interested mainly in optically thick, radiation bounded clouds that are most efficient in reprocessing the central source radiation. We assume an r^{-1} gravitational potential and escape velocity of $v_{\rm esc}/c = (3 \times 10^{13} M_8/r_{\rm cm})^{1/2}$, where M_8 is the central mass in units of $10^8\ M_\odot$. It is probably a good assumption to take the cloud velocity as the virial velocity $V_{\rm vir}$ at all r, because if clouds at very small distances had velocities much greater than that, they could escape to infinity with the same large velocity. Passing through the BLR, they would show profiles broader than observed (see § IV*c*[ii]).

A major point of concern in this simplified picture is whether the clouds maintain their identity as they move through the (hypothetical) intercloud medium. This depends on the pressure, drag, and tidal forces, and is still an open question. The changes of the cloud column density and optical depth, as a function of r, is thus a major uncertainty in any calculation which attempts to model the three-dimensional nature of the BLR. The minimal set of assumptions we use is that the clouds are dust-free, have a uniform chemical composition, and are illuminated by an isotropically emitting central source. Under these circumstances, the radial dependence of the line and continuum emission from the $r < r_{\rm BLR}$ gas is govened by the pressure and the covering factor.

a) Pressure

It is customary to assume some confining medium in pressure equilibrium with the clouds. The pressure of the intercloud medium is a lower limit to the pressure of a cloud. Individual clouds have higher pressure if, for instance, they result from transient shocks, mass loss from stars, etc.

The standard picture, as developed, for example, by Krolik, McKee, and Tarter (1981), is that the intercloud gas is at the Compton temperature. $T \geq 10^8$ K is required if the intercloud gas is stationary and the clouds are not to move through this medium supersonically. Recently, Fabian *et al.* (1986) and Mathews and Ferland (1987) showed that such high temperatures are not compatible with the observed X-ray, ultraviolet, and infrared fluxes of AGNs. The hot phase gas, if present, would be cool and opaque (Kallman and Mushotzky 1985), and the BLR clouds would not be stable against drag forces. Alternatives, such as magnetic pressure confinement (Rees 1987) and transient high-density clouds (Krolik 1988), have been proposed, and there are other possibilities. This is one of the outstanding problems in AGN study.

It is not our intention to study the confinement problem here. Instead, we assume some simple pressure laws that can describe the high-density clouds and may or may not equal the intercloud pressure. For the pressure, P, we take

$$P = r^{-s}\,, \tag{1}$$

and investigate the consequences of this assumption. In general, s may depend on r, but we do not consider this extra complication.

The natural scaling law for a gas at the virial temperature is for $s = 5/2$. However, the temperature of an intercloud medium may not equal $T_{\rm vir}$ (for example, it may be at the Compton equilibrium temperature). For $r < (m_e/m_p)R_{\rm S}$, $T_{\rm vir}$ is so high that the electrons would be relativistic; the cooling is then more effective. This suggests that $s = 3/2$ may be a better guess for smaller r. The natural scaling for a magnetic pressure gives $s = 5/2$ in an accretion flow and $s = 2$ in a relativistic wind. The presence of any 10^4–10^5 K clouds at small r requires a density high enough that bremsstrahlung and bound-free cooling dominates Compton heating, i.e., $P > P_{\rm min} \propto r^{-2}$. Provided that $P > P_{\rm min}$ at all r, the simplest model is one in which clouds maintain their identity, but merely change their density, and perhaps shape, as they fall in. This can be used to make some simplified assumptions about the size of the high-density clouds.

Denote by $\sigma(r)$ the cross section of the cloud, which depends on its pressure and shape, and assume

$$\sigma(r) \propto r^x\,. \tag{2}$$

For spherical clouds we obtain

$$\sigma(r) \propto P^{-2/3} \propto r^{2/3s}\,, \tag{3}$$

where we have neglected the temperature dependence of the clouds on P and r.

b) Covering Factor

The covering factor of the high-density clouds determines the fraction of the central source radiation absorbed and reprocessed. In principle, it is a purely geometrical factor, since we are interested in clouds with a column density large enough

to absorb the ultraviolet radiation of the central source completely. This is not trivial, since the column density of the ionized gas increases as the cloud moves in, and the ionization parameter can change as well (see § III below).

We define $C(r)$ as the cumulative covering factor up to radius r. If there is a fixed population of clouds, preserving their identity as they fall in, move out, or swirl inward as part of some disk-like flow, then

$$dC(r) \propto r^{-2} r^{1/2} \sigma(r) dr , \quad (4)$$

where the first term is the total surface area and the second is due to the motion of the cloud. Combined with the assumption on $\sigma(r)$, we obtain

$$dC(r) = r^{x-3/2}\, dr . \quad (5)$$

The more interesting cases are those with $\frac{1}{2} \leq x \leq 1$, where the contribution to the emission lines is from a large range of radii.

Note here that *we neglect obscuration*; this is not justified for large values of $C(r)$. Also, the assumption of conserved cloud numbers may well be wrong if the mass of clouds is small compared to that of the confining medium. A cloud falling in may break up, for tidal or other reasons, into smaller ones, which will tend to increase $C(r)$ at small r.

To illustrate some of the possibilities consider the following cases:

1. Clouds are in pressure balance with external medium but stay spherical as they move in or out. In this case, $C(r) \propto r^{2/3s-1/2}$, and the covering factor for small r is small if $d > \frac{3}{4}$.

2. Clouds are in radially free fall and are tidally distorted. Here $x = 2$ and $C(r) \propto r^{3/2}$. There is very little contribution from clouds at small r.

3. Clouds are magnetically confined in "tubes" of circular cross section or are aligned along a poloidal field. The cloud length is proportional to r and the diameter to $B^{-1/2} r^{-1/2}$ (if there is no flux in the cloud and its pressure balances the full stress of the field outside). In this case, $\sigma(r) \propto$ (length) $\times$ (diameter) $\propto r^{1/2+(5/4 \text{ or } 1)}$; i.e., $x = 1.5$–1.75 and $C(r) \propto r^{1 \text{ or } 1.25}$. Again, the contribution of small r clouds to $C(r)$ is small.

Obviously, there are many possibilities, and it is best to consider the observational constraints to try to find the dependence of $C(r)$ on the pressure (or vice versa). For this, we calculate a full grid of models for several chosen pressure laws, covering values of r, down to radii of high densities, where the clouds are mainly continuum sources. Several possible $C(r)$ are then used to construct a model of the ensemble and confront it with observations of AGNs. This approach could then address the question, what is the smallest radius contributing significantly to the observed spectrum?

The models we choose to investigate are those of spherical clouds in pressure balance with the external medium, and three possible pressure laws: $s = 1$, 3/2, and 2. We neglect the temperature dependence and assume that the cloud density N depends on s as in equation (1):

$$N \propto r^{-s} . \quad (6)$$

The column density of the clouds is given by

$$N\, dl \propto r^{-2/3s} , \quad (7)$$

and the ionization parameter is given by

$$U \propto r^{s-2} . \quad (8)$$

This, together with the velocity and the value of N at some distance r, uniquely defines the conditions across the BLR, for a system of clouds that is moving inward or outward.

III. PHOTOIONIZATION AT HIGH DENSITIES

The theory of photoionization equilibrium at "nebular" densities (i.e., $N < 10^{10}$ cm^{-3}) has been well developed over the past decades (see, for example, Osterbrock 1988). Indirect arguments, based on the observed carbon spectrum, suggest that BLR clouds are generally characterized by densities $\sim 10^{10}$ cm^{-3} (Davidson and Netzer 1979), although the hydrogen lines may require that a denser region also contribute (Collin-Souffrin and Dumont 1986; Hubbard and Puetter 1985). The extension of conventional photoionization codes to densities approaching a stellar atmosphere is a major aim of this paper. Among the major concerns are the following: (*a*) the radiation density is high, so that line transfer strongly affects the level populations and emergent spectrum; (*b*) the particle density is high, so that collisional effects, such as collisional ionization and three-body recombination, are important; (*c*) continuous optical depths can become significant; examples include the Balmer and Paschen, free-free and H^- absorption in the infrared; and (*d*) enough physics to go to the LTE limit should be incorporated. In many respects, the goal is to be able to approach stellar atmosphere conditions from the nebular limit.

This work presents calculations which were performed with two independent codes, "Cloudy," most recently described by Ferland and Rees (1988), and "ION," most recently described by Netzer (1987). Although the codes were developed independently, they have many underlying physical assumptions in common. We have made several detailed comparisons of the codes, under a variety of conditions, to verify the accuracy and consistency of the two. In the following discussion, we will outline methods, processes, and assumptions employed by the codes in general terms. This is not intended as a formal statement of exactly how either code works, but rather is a general outline of the physics each code attempts to incorporate. In some cases, the description is true of only one of the codes, the one making the most complete simulation of the physical process in question. In these instances where the codes differ, we have checked that this does not cause significant differences in the emergent spectrum.

a) Radiative Transfer

Radiative transfer effects affect the thermal equilibrium of the gas when the collision time scale approaches an effective lifetime $\tau \sim (A_{ul}/N_{scat})^{-1}$, where A_{ul} is the transition probability and N_{scat} is the number of scatterings a line photon undergoes before escaping. For permitted metal lines (which often have optical depths $\sim 10^4$), line thermalization becomes important at densities $N > 10^{12}$ cm^{-3}; these effects are important for hydrogen at considerably lower densities.

Two approaches to this problem can be identified: the first is to treat the radiative transfer in detail, at the expense of the atomic physics; the second approach is to treat the atomic physics in detail, at the expense of the radiative transfer. A formal treatment of both line transfer and the microphysics is to be preferred, but it will be some time before such a simulation can be performed. Among the radiative transfer approaches, Avrett and Loeser (1988; hereafter AL) consider a five-level hydrogen atom, assume LTE for helium, and use a coronal equilibrium cooling function for the heavy elements.

Hubbard and Puetter (1985) also treat a five-level hydrogen atom, but neglect helium and heavy-element cooling and opacity entirely. The atomic physics approach, which we take here, attempts to simulate the physical processes in detail but treats the radiative transfer locally, using a version of the escape probability formalism (see, for example, Kwan and Krolik 1981; Elitzur 1984). Collin-Souffrin and Dumont (1986) attempted a more complete solution, but many lines were still treated with the escape probability method. Roughly 200 optically thick lines are treated in the present paper; this would not be possible using a more formally correct approach to the radiative transfer.

It is not clear whether one approach is to be preferred over the other; AL find that the escape probability method does reproduce the exact radiative transfer results for hydrogen within a factor of 2. Metal lines, which are important coolants and hence are governed by energy conservation, would probably agree better. The simplifications to the ionization and cooling of helium and the heavy elements AL made in order to do the radiative transfer correctly make the calculation quite different from typical AGNs. Emission lines of the heavy elements and helium provide clues to the conditions within the BLR which *are at least as important* as the hydrogen lines, and we put great emphasis on the accurate calculation of these lines. We accept that some of the line predictions presented in this paper (most likely the weaker ones) are likely to be in error by factors of 2.

i) *The Escape Probability Function*

At low densities, line scattering for a two-level atom is coherent in the atom's reference frame, and the line profile function is described by the incomplete redistribution function. At high densities, the Stark effect can broaden the line, while, when the radiation density is high, scattering within excited states can broaden reasonance lines such as Lyβ (line interlocking), destroying the coherence of the scattering process. In this case, complete redistribution describes more closely the scattering process.

In this paper, we use three escape probability functions. For metal lines such as C IV λ1549, the Lyα transitions of hydrogen and helium, and He I λ10830, we assume incomplete redistribution. Two recent studies of line formation in the context of this approximation are those of Bonilha *et al.* (1979) and Hummer and Kunasz (1980). Both studies suggest escape probabilities of the form

$$\beta_{\rm inc}(\tau) = [1 + b(\tau)\tau]^{-1} , \tag{9}$$

but there is substantial disagreement in the form and value of the factor $b(\tau)$, sometimes by more than a factor of 2. (This is after due allowance is made for the different definitions of optical depths in the two papers.) We use the Hummer and Kunasz results, which we approximate as

$$b(\tau) = 1.6 + \frac{3(2a)^{-0.12}}{1 + a\tau} \qquad (a\tau > 1) , \tag{10}$$

$$b(\tau) = 1.6 + \frac{3(2a)^{-0.12}}{1 + (a\tau)^{-1/2}} \qquad (a\tau < 1) , \tag{11}$$

where a is the damping constant. The numerical calculations extend only to values of a larger than $\sim 10^{-4.34}$. Intercombination lines such as C III] λ1909 become optically thick, but have much smaller damping constants. Accordingly, we do not allow $b(\tau)$ to become larger than 5; the exact value of $b(\tau)$ is in fact quite important at high densities, when lines are collisionally deactivated.

For all hydrogen lines other than Lyα, we assume complete redistribution:

$$\beta_{\rm com}(\tau) = [1 + b(\tau)\tau]^{-1} + 0.25(a/\tau)^{1/2} , \tag{12}$$

with $b(\tau)$ given above. This is the form suggested by Canfield *et al.* (1984) and Collin-Souffrin and Dumont (1986).

If τ is the optical depth in the direction toward the source of ionizing radiation and T is the total optical depth, then the escape probability entering the balance equations is

$$\beta(\tau, T) = [\beta(\tau) + \beta(T - \tau)]/2 . \tag{13}$$

All of the calculations are the result of *at least* two iterations over the whole cloud, to ensure that the optical depth scale is well defined.

Distant collisions with charged particles broaden the upper level of resonance lines, and, in the limit of very high densities, this will make the scattering process completely noncoherent. We closely follow the treatment of Puetter (1981) in our handling of Stark broadening and the calculation of the Stark escape probability β_S. For lines described by incomplete redistribution, we define a total escape probability $\beta_{\rm eff}$ given by

$$\beta_{\rm eff} = \min (\beta_{\rm inc} + \beta_S, \beta_{\rm com}) . \tag{14}$$

The total effective escape probability is not allowed to exceed the complete redistribution value for $\tau > a^{-1}$. Optical depths and escape probabilities are computed for *all* permitted and intercombination lines; for the extreme conditions considered here, the cooling can be distributed among many lines.

A wide range of models was computed in which the form of the escape probability was altered to simply $(1 + 1.6\tau)^{-1}$ for incomplete redistribution, and to the form appropriate for Hα for complete redistribution. The largest effect was seen in the physical conditions in the partially neutral zone. The neutral fraction changed by roughly 15%, and some hydrogen line fluxes changed by nearly 50%. This underscores the importance of choosing the correct form of the escape probability function in these calculations.

ii) *Line Continuum Overlap*

One powerful asset of the escape probability formalism is that it is relatively straightforward to include the effects of line fluorescence and continuum overlap (Elitzur and Netzer 1984; Netzer, Elitzur, and Ferland 1985, hereafter NEF85). We consider the He II–O III Bowen fluorescence mechanism (see § III*c*[ii]) along with O I–Lyβ fluorescence. For line destruction by continuous opacity (i.e., ionization by line photons), we include the ground and excited states of hydrogen, He^0 $2\,^1S$ and $2\,^3S$, and the following lines: Lyα, Hα, Pα, He I λ584, He II λ304, Mg II λ2798, and the ultraviolet Fe II lines. We use equations (1)–(6) from NEF85, modified as follows.

The effective escape probability used to calculate the level populations in cases of line-continuum overlap is

$$\beta_{\rm eff} = X_c + X_l \beta_{\rm lc} , \tag{15}$$

where

$$\beta_{\rm lc} = \beta(\tau_{\rm line} + \tau_{\rm continuum}) , \tag{16}$$

$$X_c = \frac{\kappa_c}{\kappa_c + \kappa_l} , \tag{17}$$

and

$$X_l = \frac{\kappa_l}{\kappa_c + \kappa_l} . \quad (18)$$

The emergent line flux is

$$N_{u,l} A_{u,l} \beta_{lc} \exp(-\tau_{in}) \frac{h\nu}{4\pi} (\text{ergs cm}^{-3} \text{ s}^{-1} \text{ sr}^{-1}) , \quad (19)$$

and the number of continuum absorption (i.e., ionizations) is

$$N_{u,l} A_{u,l} [X_c(1 - \beta_{lc}) + \beta_{lc}[1 - \exp(-\tau_{in})]\} . \quad (20)$$

The extra reduction in the line flux due to the $\exp(-\tau_{in})$ factor, where τ_{in} is the continuous optical depth at the line frequency in the direction toward the source of ionizing radiation, improves the agreement with the numerical calculations of Hummer and Kunasz (1980) in the limit of large continuous optical depth. We do not add the equivalent factor of $\exp(-\tau_{out})$, because it is not very clear how such photons are scattered. Thus, the intensity of many lines with $\lambda < 912$ Å is rather uncertain.

b) Hydrogen

i) The Hydrogen Atom

Hydrogen provides a major heating, cooling, and opacity source, and must be treated with great precision if meaningful results are to be obtained.

The hydrogen atom we adopt attempts to account for physical processes affecting levels up to $n = 100$. In the calculations presented below, it is mainly the ground and first excited states which affect the heating, cooling, and opacity of the cloud. Nonetheless, the more highly excited states must also be treated with precision, since the ground-state population can only be computed reliably when populations of excited levels are also known. This is because the majority of the populations of the ground state are the result of capture cascades to the ground. Computing the full set of level populations for the hydrogen atom is a well-known problem; the most troublesome aspect is that many hundreds of levels must be included if an accurate solution is desired. As an example, the total recombination coefficient is the result of the sum to infinite principal quantum number (in the limit of low densities). It is not correct to increase simply the radiative recombination coefficient of the highest level considered to include the contribution from the neglected levels, since collisional processes can ionize highly excited levels before cascade to the ground state occurs. Thus, a solution to the population of the ground state is inextricably interwoven with the problem of determining the physics of the highly excited levels.

Unfortunately, it is only practical to treat a dozen or so levels per ion in the types of ionization–thermal equilibrium codes used in this paper. For example, Kwan and Krolik (1981) used six levels only; AL use five. We approximate the physics of the highly excited levels by replacing levels above some principal quantum number by a few pseudostates, with properties set by averaging over increasingly larger groups of true levels. We model the hydrogen atom as a 10-level system (Cota 1987). Levels below seven or eight are treated in the same manner as in the true hydrogen atom, and three pseudostates are incorporated to mimic the radiative and collisional properties of all levels up to $n = 100$. For the conditions of interest here, the higher of these levels are controlled by collisions and are close to LTE; as a result, they populate low-lying levels mainly through collisional and radiative relaxation. This scheme has been compared with the case B calculations of Hummer and Storey (1987) and have been found to be in excellent agreement. A detailed description of the averaging over these pseudostates is given in Cota (1987); the detailed breakdown of principal quantum number is not the same in the two codes used here and does not affect the results.

We define the neutral hydrogen density to include the populations of all excited levels when setting the free electron density from charge conservation. At densities of interest here, pressure shielding reduces the ionization potential of the atom to include some of the levels grouped into the highest supplementary level when $N_e \sim 6 \times 10^{13}(T_e/10^4)$ cm^{-3} (Mihalas 1978). The statistical weight of this level is large and its population can be significant at high densities. We correct for this effect by solving for the highest bound level,

$$n = 120\left(\frac{N_e}{10^{13} \text{ cm}^{-3}}\right)^{-1/4}\left(\frac{T_e}{10^4 \text{ K}}\right)^{1/4} , \quad (21)$$

and lowering the statistical weight of the highest pseudostate accordingly.

ii) Physical Processes

Level populations for hydrogen are determined by solving the usual system of equations of statistical equilibrium (see, for example, Mihalas 1978; Avrett and Loeser 1988). The processes included are the following:

1. *Photoionization, induced recombination.*—Photoionization cross sections for the lowest seven levels are from standard references (see Mihalas 1978). Induced recombination is important for the higher levels and is included (Krolik and McKee 1978; Ferland and Rees 1988). The three supplemental levels are assumed to be collisionally controlled, and photoionization is neglected. Paschen and higher continua are assumed to be optically thin. Paschen continuum optical depths never exceeded 0.1 in the calculations presented below.

The Lyman and Balmer continua are treated with optical depths. including stimulated emission. The incident continuum is attenuated by an optical depth given by $d\tau_n(\nu) = \kappa_n(\nu)(N_n - N_c g_n/g_c)dr$, where the factor in parentheses is the correction for stimulated emission and the symbols represent the optical depth, opacity, and populations of the lower level and the continuum. Recombination coefficients to the $n = 1$ and $n = 2$ levels are written as $\alpha_i \eta_i$, where η_i is a recombination efficiency, for example:

$$\eta_1 = \{\exp(-2\tau_{912}) + \exp[-2(T_{912} - \tau_{912})]\} , \quad (22)$$

where τ_{912} is the optical depth at 912 Å in the direction toward the source of ionizing radiation, and T_{912} is the total optical depth through the cloud. The extra factor of 2 accounts for oblique escape of ionizing diffuse photons. The code "ION" includes a more sophisticated treatment of the Balmer continuum (Wills, Netzer, and Wills 1985), but the differences are found to be small over the typical range of $\tau_B < 3$ investigated in this paper.

2. *Free-free heating, cooling.*—The free-free opacity of dense clouds is large in the infrared, where AGNs are known to emit a great deal of radiation. As a result, free-free heating is an important heating source for deep regions of the denser clouds we consider here. The codes bin the near-infrared ($\lambda < 100$ μm) continuum and treat the opacity and heating rate bin by bin. Both codes use Gaunt factors from Karzas and Latter (1961), and define a cutoff frequency ν_{cut} where the cloud becomes

optically thin to free-free absorption. The free-free cooling is then approximately

$$\Lambda_{ff}(\tau) = \Lambda_{ff}(\tau = 0)[\exp(-h\nu_{cut}/kT)], \quad (23)$$

where $\Lambda_{ff}(\tau = 0)$ is the free-free cooling in the optically thin limit.

3. *Collisional ionization, three-body recombination.*—Collisional ionization cross sections for the lowest quantum numbers are taken from the compendium by Janev *et al.* (1987). Collision data for highly excited levels are taken from Vriens and Smeets (1980), which is based on more recent experimental data than Johnson (1972). These latter cross sections are uncertain by something like a factor of 2. Tests show that the effects of changes in the collisional ionization cross sections do not change the predictions presented here by a great deal. Three-body recombination rates are derived from collisional ionization rates and detailed balance arguments. Rates for the supplemental levels are derived by averaging over the rates for each level, assuming that the highly excited levels are in LTE at 10^4 K. This is a good approximation when the density is high enough for collisions to affect significantly the equilibrium of these levels.

4. *Collisional excitation, de-excitation.*—Collisional excitation rates from the ground to the first two excited states are taken from Callaway (1988). These rates are in good agreement with those of Aggarwal (1983). Collisional rates between $n = 2$ and 3 are taken from Callaway (1988). All other rates are from Vriens and Smeets (1980). Uncertainties in these latter rates affect some lines, such as Pα, at the 20% level. Rates for the supplemental levels are derived by averaging over populations assuming LTE at 10^4 K.

5. *Diffuse ionization mechanism.*—In addition to photoionization by the primary continuum, we include photoionization of excited-state hydrogen by several lines. Photoionization of the $n = 2$ level by Lyα, Mg II λ2798, and the Fe II ultraviolet lines, the $n = 3$ level by these lines and Hα, ionization of $n = 4$ by Lyα and Hα, and $n = 5$ by Lyα, Hα, and Pα. The formalism described earlier is used.

A recent paper by Zheng (1989) discusses such processes in hydrogen and suggests that they can greatly influence the ionization balance and emergent line fluxes. Tests performed on several of the models described below do not show a very significant effect.

c) *Helium*

i) He I

Feldman and McAlpine (1978) and Netzer (1978) calculated intensities of some He I lines in AGNs, using 10–11 level atoms and the standard escape probability approach. Kwan and Krolik (1981) and Kwan (1984) used a simplified two-level atom in their models. Netzer (1978) suggested that the intensity of He I λ5876 is proportional to the ionizing flux, thus BLR clouds closer to the central source produce stronger lines. Kwan (1984) investigated the same process and extended the calculations over a larger range in ionizing flux. Some AGNs show He I λ5876 which is much broader than Hβ (Shuder 1982), thus the He I lines may provide the best indication that smaller distances correspond to larger cloud velocities. An extreme example of the enhancement of He I λ5876 can be found in Netzer (1987) for a model involving a nonisotropic radiation field of a thin accretion disk. Some of the high-density clouds considered there produce He I 5876 actually stronger than Hβ.

The above mentioned calculations were not intended for densities much greater than 10^{10} cm^{-3}. In particular, they do not take a full account of collisional ionization and three-body recombination that are important for the line intensity and the ionization equilibrium. In addition, there are new calculations of collision strengths for the $n = 2$ and $n = 3$ transitions (Berrington and Kingston 1987) that may change some of the older results. The recent calculations by Almog and Netzer (1989) include the new cross sections and take into account all processes thought to be important at $N_e \leq 10^{14}$ cm^{-3}. The calculation includes all levels up to $n = 100$ where some levels (up to $n = 12$) are considered individually and others are grouped into four fictitious levels, similar to the treatment of the hydrogen atom described here. Collisional ionization and three-body recombination are included with hydrogenic rates, and the line transfer treated with the local escape probability method. Deviations from the older results are quite large for $N_e > 10^{11}$ cm^{-3},

Almog and Netzer (1989) suggested a simplified 16-level scheme which can be easily incorporated into existing photoionization models. The scheme consists of three singlet and 13 triplet levels where the four upper ones represent all $5 \leq n \leq 100$. The reduced scheme reproduces, quite accurately, the intensity of the lines and the net recombination rate (three-body minus collisional ionization) of the more detailed calculations and is most suitable for the present work. Additional processes that we consider are the ionization of hydrogen by He I 584 and the absorption of H Lyα by the He I $2\,^3S$ level.

ii) He II

Calculations of the He II spectrum are complicated, because of the scattering of the He II Lyα line photons that can ionize hydrogen and He^0, and excite O III (the Bowen fluorescence). There are several low-density calculations for both the He II recombination spectrum (Brocklehurst 1971; Seaton 1978) and Bowen fluorescence (Weymann and Williams 1969; Harrington 1972; Saraph and Seaton 1980; Kallmann and McCray 1980) and extensive, high-density ($N \leq 10^{12}$ cm^{-3}) case B calculations for He II by Hummer and Storey (1987). Discussion of the He II spectrum of AGNs is given in Netzer and Davidson (1979), MacAlpine (1981), and Grandi (1983), and high-density calculations for He II and the Bowen fluorescence lines are described in Eastman and MacAlpine (1985) and NEF85.

Of all calculations applicable to AGNs, only NEF85 incorporate the O III line solution into a multilevel scheme for He II. These authors describe a method, based on escape probabilities, that incorporates fluorescence and the overlapping of lines and continuum simultaneously with the ionization equilibrium equations. This is crucial, since the Bowen lines and the He II Lyα intensity critically depend on the O III/He II abundance ratio. The results are in good agreement with those of more sophisticated transfer calculations. As already mentioned, the treatment of line and continuum overlapping in this way is simple and quite accurate. It is especially important for the calculation of the ionization of hydrogen by the He II, O III λ304 line which is one of the major uncertainties in calculating the ionization equilibrium of the BLR clouds (Netzer and Ferland 1984). The Eastman and MacAlpine (1985) transfer method is somewhat more accurate but is limited, since the separation of the ionization and the transfer equations becomes quite complicated. Those authors were not able, therefore, to investigate much of large parameter space, or the strength of He II lines other than Lyα.

The present calculations employed the NEF85 treatment of the 304 Å line, as well as the solution of the intensity of the He II and O III Bowen lines, as described in NEF85, but including many more He II levels. It is currently a 10-level plus continuum scheme, with seven real and three fictitious levels, representing all levels up to $n = 100$, in a way similar to the treatment of the hhydrogen atom. The level $2\,^3P^0$ of O^{++} (the upper level of the O III λ303.799 line) is included as an additional level, and its population is found simultaneously with those of the He^+ levels. We also consider optical depth effects in all of the He II lines, the interaction of the 2–4 He II transition with the H Lyα radiation field (see NEF85), and the ionization of hydrogen by the He II Lyman lines.

Hummer and Storey (1987) calculated the spectrum of ionized helium under generalized case B conditions; i.e., large optical depth in the Lyman lines, no optical depth in other lines, and all collisional transitions *except* for collisions to and from levels 1 and 2. We have made an extensive comparison of those calculations and ours and found very good agreement for all He II lines over the entire range of $10^6 < N_e < 10^{13}$ cm^{-3}, with typical deviations of only a few percent. The most extreme deviations are less than 15%, and the reason for the disagreement is probably the different collisional data used (we used the Bates 1962 data). These differences occur only at very high densities and are well within the uncertainty in the collision strengths. The present 10-level He^+ atom is thus a good, accurate method to calculate the He II spectrum for all densities up to 10^{13} cm^{-3}.

d) The Heavy Elements

Lines of the heavy elements provide a major constraint on conditions with the BLR. For instance, the fact that C III] and C IV lines usually have very similar intensities relative to Lyα suggests that conditions within the BLR somehow "adjust" themselves to accommodate the wide range of luminosities encountered in the AGN phenomenon (Davidson 1977). The agent adjusting these conditions has still not been identified.

It has long been known that the familiar ultraviolet emission lines of quasars are those produced by moderately ionized gas at a density of $\sim 10^{9.5}$ cm^{-3} (see, for example, Davidson and Netzer 1979). Intercombination lines, such as C III] λ1909, are collisionally deactivated at higher densities, and strong resonance lines such as C IV λ1549 are thermalized at densities above $\sim 10^{12}$ cm^{-3}. These lines are major coolants for the gas, so the tendency is for clouds to grow hotter as the density increases and cooling efficiency decreases, if the ionization and heating are kept constant. The result is that other lines, generally electric dipole transitions further in the ultraviolet such as C III λ977, become strong. As a result, the cooling function is no longer dominated by only a few lines, as is the case at conventional BLR densities. We include at least one (and usually more) permitted transition for all low and moderate stages of ionization of the heavy elements in these calculations. All lines are treated with full optical depth effects, including intercombination lines, although such lines as C III] λ1909 do not become very optically thick in the calculations presented here.

The customary treatment of the heavy-element ionization balance includes only two levels, continuum and ground state (see, for example, Osterbrock 1988). A net recombination coefficient, which is a sum over all levels, is used. This is a poor approximation for high densities, because recombinations to excited levels do not necessarily result in population of the ground state; collisional or photoionization can occur. Three-body recombination is increasingly important for densities exceeding 10^{10} cm^{-3}, and its effects must be included if a correct approach to LTE is desired. We use new results by Cota (1987), who calculated the net recombination rate (three-body recombination less collisional ionization) for all charges, assuming hydrogenic levels. These give a good first-order estimate of the above processes, for $N_e \leq 10^{13}$ cm^{-3}, and represent a major improvement in the computation of the ionization balance at high densities.

Finally, we take great care in evaluating all X-ray related processes (Auger and inner shell ionization; secondary collisions by suprathermal electrons; Compton scattering of both free and bound electrons; pair production in the electric field of the nucleus). The collisional ionization of heavy elements by secondary electrons is treated using the Shull and Van Steenberg (1985) rates scaled from hydrogen by the relative collision cross section (Lotz 1967).

The specific abundances used here are 10^5 (He: C: N: O: Ne: Mg: Al: Si: S: A: Ca: Fe:)/H = (10^4: 47: 9.8: 83: 10: 4.2: 0.27: 4.3: 1.7: 0.38: 0.23: 3.3), and are basically solar values. It may be argued that under the extreme conditions of high densities and large optical depth lines of less abundant elements are important coolants. We have not investigated this in detail, but suspect that this will not add much to our understanding of AGNs for two reasons: first, we are not aware of a strong emission line of an element other than the ones on the above list. Second, cooling by free-free and other diffuse continua are likely to be more important even at the conditions considered by us.

IV. RESULTS

a) Continuum, Ionization, Parameter, Geometry, and Density

The ionizing-heating continuum must be carefully defined over all energies which interact with matter. This includes not only the "classical" ionizing radiation field (i.e., $h\nu > 13.6$ eV), but also softer radiation, which ionizes hydrogen and helium in excited states and heats the gas via free-free and H^- absorption.

With one exception, the ionizing continuum is that deduced by Mathews and Ferland (1987). The infrared continuum has an energy slope of -1 (i.e., $f_\nu \sim \nu^{-1}$) for wavelengths shortward of 10 μm; for wavelengths between 10 μm and 1 mm, the slope is $f_\nu \sim \nu^2$. This is chosen to prevent runaway free-free heating at the surface of the cloud as a result of submillimeter radiation. The continuum has the "mean" observed slope in the ultraviolet and X-ray and is normalized to give a proper value of α_{ox}. It is chosen to be consistent with the observed ratio Lyα/He II λ1640 (with "standard" model parameters) and is consistent with the soft X-ray observations of Wilkes and Elvis (1987). The γ-ray continuum changes slope at 100 keV to be consistent with γ-ray background observations. The "big bump" peaks at roughly 60 eV; tests show that the precise position of the peak of the big bump affects the predicted emission-line spectrum more than similar uncertainties in other regions of the spectrum because radiation at this energy is very efficient at interacting with matter (see also Krolik and Kallman 1988).

We use only this continuum in this work. The reasons are several; there are already a vast number of free parameters, and the consideration of more than one continuum would complicate matters further. Observationally, the emission-line spectrum does not seem to be sensitive to details about the exact continuum; apparently the emission-line clouds accom-

modate different continua (both shape and luminosity) by "adjusting" their densities to produce similar emission-line ratios (see, for instance, Baldwin and Netzer 1978). Physically, it is difficult to understand how to compare two models heated by different continua to determine the effects these differences make. For instance, should calculations with the same ionization parameter as defined by the ratio of ionizing photon to hydrogen densities be compared, should another ionization parameter defined relative to the flux density at 912 Å (i.e., Davidson 1977) be kept constant, or does the "same" cloud exposed to different continua keep something else constant, such as radiation pressure, 10 μm flux, etc.? Here, we will be concerned mainly with overall features of the calculations, such as the behavior of ionized gas at high densities. Our conclusions are not sensitive to moderate changes in the continuum.

We use fairly standard assumptions concerning the geometry of the BLR. Studies of the Lyman limit show that the covering factor is small (Smith *et al.* 1981; Carwell and Ferland 1988), so the BLR is assumed to be highly clumped. The ionization parameter can change across the BLR (eq. [8]), but we must normalize it at some distance. The aim of this paper is to investigate high-density BLRs, and we have chosen to normalize U such that its value at the distance where $N = 10^{10}$ cm^{-3} is 10^{-2}; i.e., close to the one used in previous calculation of this kind. Given such parameters, the clouds are readily shown to be small relative to the distance to the central object. In this case, a plane parallel geometry, which we use, is appropriate. The clouds have constant density, in keeping with our desire for simplicity. Tests show that constant pressure clouds give the same tendencies. The overall geometry is spherical, and the number of clouds per unit volume at a given distance, or the differential covering factor, is determined by the scaling laws described in § II. The parameters (distance, ionization parameter, radius) are gven below.

b) Line Intensities versus Density: Model A

We consider first in detail one set of models, for one cloud with a constant column density ($N = 10^{23}$ cm^{-3}) and ionization parameter ($U = 10^{-2}$), to demonstrate the physics of clouds at a wide range of densities. The results are not sensitive to the chosen column density, and the ionization parameter was chosen in our hope of reproducing the C III] λ1909/C IV λ1549 intensity ratio. We chose not to list the Fe II intensities since the calculation we are performing uses a simplified scheme, as suggested by Wills, Netzer, and Wills (1985). As noted by these authors, this approximation has not been tested at very high densities. The problem of Fe II emission under such circumstances is currently under study (Netzer 1980, in preparation).

Figure 1 shows normalized line intensities, the ratio of the emergent intensity over the density (ergs cm s^{-1}). This ratio will tend to be constant for lines that are not collisionally de-excited, because it is proportional to the covering factor. Table 1 lists detailed line predictions for densities of 10^{10} and 10^{12} cm^{-3}.

The predictions fall into four broad groups. Optically thick

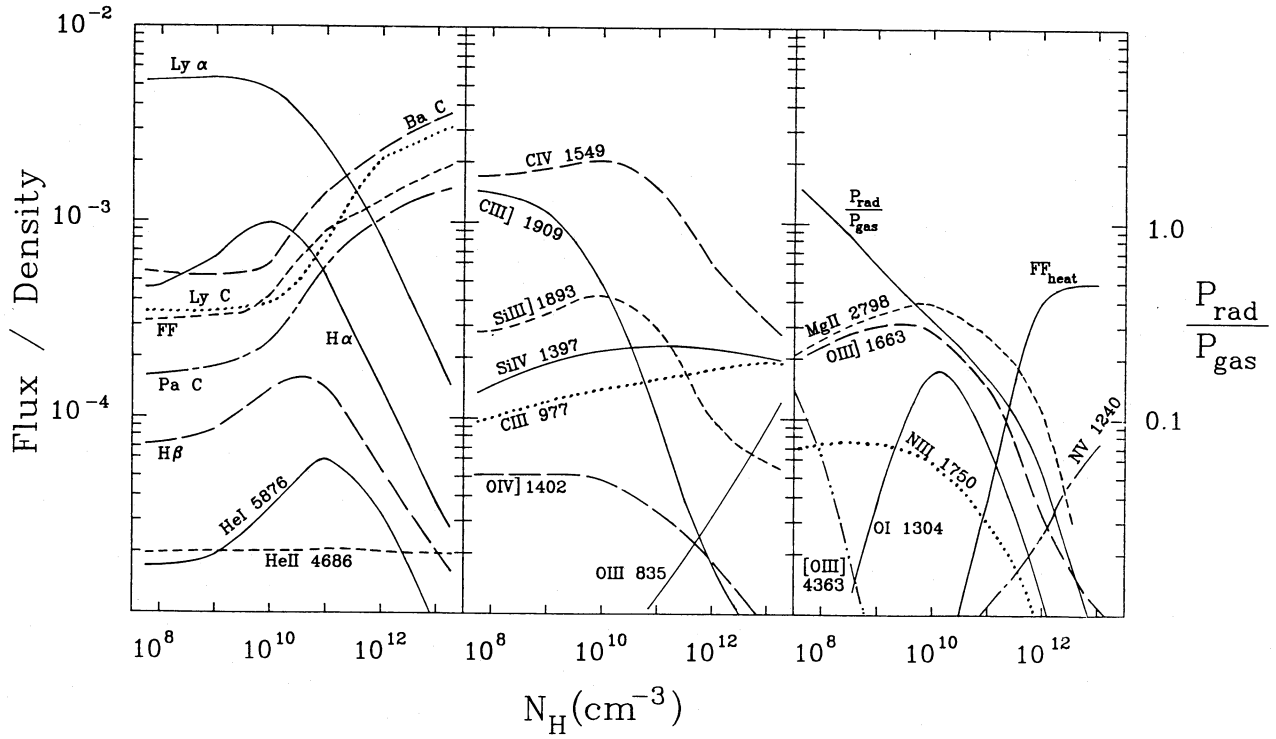

FIG. 1.—Series of calculations in which the density was varied but other parameters held constant. Column density is 10^{23} cm^{-2}, and ionization parameter is $U = 10^{-2}$. Curves show the ratio of the surface flux (ergs cm^{-2} s^{-1}) to the total hydrogen density (cm^{-3}), so that lines radiating with 100% efficiency throughout (such as He II λ4686) have flat curves. In general, lines become weaker at very high densities as the result of thermalization; this cooling is then radiated largely as continua. Largest ratio of radiation to gas pressure which occurred in the calculation, computed as in Elitzur and Ferland (1986), is shown in the rightmost panel.

TABLE 1

MODEL A[a]

Line	$N = 10^{10}$ cm^{-3}	$N = 10^{12}$ cm^{-3}
Lyα	33	16
Hβ	1	1
Hα	6.5	2.8
Pα	0.71	0.15
LyC	2.6	34
Ba C	4.2	47
Pa C	1.7	21
$f - f_{cool}$	2.7	25
He I λ5876	0.23	0.60
He II λ4686	0.15	0.48
He II λ1640	1.29	4.25
C II λ1335	0.31	1.31
C II] λ2326	0.46	0.042
C III λ977	1.0	3.6
C III] λ1909	3.5	0.37
C IV λ1549	14	15
N III] λ1750	0.4	0.1
N IV] λ1486	0.31	0.1
N V λ1240	0.06	0.5
O I λ1304	1.1	0.52
O I λ8446	0.18	0.09
O III] λ1663	1.8	0.63
O III λ835	0.03	0.65
O III λ3133	0.6	1.7
O IV] λ1402	0.35	0.37
Mg II λ2798	2.5	1.4
Si II λ1207	0.4	1.4
Si III] λ1893	2.8	1.8
Si IV λ1397	1.6	4.8
Hβ flux	1.47×10^6	5.34×10^7

[a] Relative line intensities for model A; $U = 10^{-2}$, Hβ flux in units of ergs s^{-1} cm^{-2}.

lines such as the hydrogen lines and C IV λ1549 initially keep fairly constant normalized intensities until densities exceed $\sim 10^{10}$ cm^{-3}, when the lines become thermalized and saturate at their blackbody limit. In this case the flux (ergs cm^{-3} s^{-1}) no longer increases, and the normalized flux falls as N^{-1}. Balmer lines increase initially in normalized intensity for densities less than 10^{10} cm^{-3}, since the flux of ionizing photons, $\phi_H = UNc$, increases. This parameter determines the population in excited states (Ferland, Netzer, and Shields 1979); collisional enhancement increases as this population increases. These lines too are thermalized when the density exceeds $\sim 10^{11}$ cm^{-3}. This behavior is also shared with helium triplet lines such as He I λ5876.

The many intercombination lines included in the calculation weaken as the density increases for basically the same reason; they become thermalized when their critical density is reached. Optical depths are included for all intercombination lines, although they seldom much exceed unity. The C III] λ1909 line is deactivated collisionally at the lowest density listed in the table.

The third group consists of high-excitation lines; these tend to become stronger at higher densities. The clouds remain optically thick to the incident ionizing continuum and must remain in thermal equilibrium. As the density increases and lines which are usually the strongest coolants are thermalized (i.e., Lyα and C IV λ1549), the gas grows hotter and an increasing fraction of the cooling is carried by high-excitation lines such as C III λ977.

Continua, such as the Lyman, Balmer, and Paschen continua, and fee-free emission form the last group, which dominates cooling at the very highest densities. At $N \sim 10^{13}$ cm^{-3}, nearly all optically thick lines are thermalized, and continuum cooling processes produce the majority of the energy loss. At the very highest densities, the clouds are efficient continuum emitters but produce little else.

Figure 1 also gives the largest ratio of radiation to gas pressure which occurred in the calculation. This is computed using assumptions described by Elitzur and Ferland (1985); Lyα provided the majority of the radiation pressure for these calculations. Radiation pressure falls at high densities as line thermalization becomes more important. Constant pressure clouds, which are supported by an external medium, would become unstable when the ratio of radiation to total pressure exceeds about 50%; for these calculations, this occurs when the density falls below $\sim 10^{9.5}$ cm^{-3}. It now seems doubtful that BLR clouds are supported by an external medium, at least one at the Compton temperature of the observed radiation field (Mathews and Ferland 1987). Other physics, such as magnetic fields (Rees 1987) or stellar envelopes (Penston 1988; Kazanas 1988; Scoville and Norman 1988), could determine the structure of the clouds, and clouds supported by such mechanisms would not be disrupted by radiation pressure.

c) *Integrated Line Intensities*

In this section, we describe the overall spectrum obtained by integrating through the cloud distributions described in § II to predict observed spectra.

i) *The Inner and Outer Boundaries*

Although the theory can outline how the cloud pressure changes with radius, it does not provide an ab initio inner or outer radius. It is still not clear what physics describes the size of the BLR; this will depend on such unknowns as the cloud production and confinement mechanisms, and is not discussed further in this paper.

The photoionization calculations do provide "empirical" limits to the radial integration, however. As noted above, clouds in pressure equilibrium with an external medium would be disrupted by radiation pressure if the density were smaller than $\sim 10^{9.5}$ cm^{-3}. The spectrum provides a more reliable estimate of the outer radius. Clouds with densities below $\sim 10^9$ cm^{-3} produce significant broad [O III] emission (see Fig. 1). Observationally, the [O III] λ4363 line has a strength less than roughly 10% of Hβ, since the line is not observed from the BLR. (The [O III] λ4363 line is predicted to be stronger than [O III] λ5007 because of its much larger transition probability.) The radial integrations described below produced too much [O III] emission if the density at the outer radius fell below $\sim 10^{8.5}$ cm^{-3}; we chose this density to set the outer radius.

We do not consider densities greater than 10^{13} cm^{-3} for several reasons. Among the more important are the following: (*a*) The heavy-element ionization balance computed by our codes is completely unreliable at higher densities; at 10^{13} cm^{-3} the recombination mechanism is predominantly three-body recombination, which is treated in an only approximate manner. (*b*) The clouds are quite optically thick in the Balmer, Paschen, and He I $2\,^3S$ continua, and to free-free absorption in the near-infrared. Transfer of radiation in these continua is only approximately treated in the present calculations. (*c*) Very

dense clouds are not efficient line emitters (Fig. 1) and, given the forms of the pressure laws we consider, do not contribute much to the net emission.

We calculate three basic models, corresponding to three pressure laws $P \sim r^{-s}$, with $s = 1$, 3/2, and 2 (see the end of § II). We neglect the temperature dependence and assume s to define also the N-r relation. All our models are for cases where clouds retain their identity as they move in or out at the free-free velocity. The ionization parameter and the column density are thus dimple functions of r and are well determined except for a normalization constant. As explained, we choose to normalize the geometry by assuming that the ionization parameter is similar to the one known to give good results at a density of 10^{10} cm^{-3} ($U = 10^{-2}$). Given this normalization, the functional forms of N and U, and the limits on the lowest and highest density, we arrive at the parameters described in Table 2. We stress that other choices of s or the normalization are possible.

ii) *Line Profiles*

Profiles of emission lines arising from various excitation and ionization potentials are a powerful probe of the stratification of the BLR. Models which include radial stratification must pass the test that profiles of such lines as Lyα, C IV λ1549, and C III] λ1909 agree to large extent (see, for example, Baldwin and Netzer 1978; Wilkes and Carswell 1982). Balmer and helium line profiles *do not* agree exactly (see Shuder 1982; Crenshaw 1986), which also is telling us about the radial structure of the BLR.

It is again necessary to adopt a velocity law for the BLR if line profiles are to be modeled. To be consistent with our previous assumptions, we assume virial equilibrium, so that $v \propto r^{-1/2}$. This velocity law holds (to within a scale factor of order $\frac{1}{2}$) for free fall, orbital motion, or chaotic motions. Of these possibilities, only the latter can produce symmetric Lyα profiles, since this line is strongly beamed in the direction of the source of ionizing radiation (Ferland, Netzer, and Shields 1979).

We assume isotropic radiation of all lines and model the profiles assuming square-shaped line profiles for each spherical shell of gas. This is a compromise between the various possibilities; orbital motion produces a saddle-shaped profile, while radial outflow can produce a logarithmic profile. We are not especially concerned with the very core of the line, because NLR contamination is expected there. We further smooth the line profiles by a boxcar average of width 300 km s^{-1}. The width of the line is set by assuming that the mass of the central object is 10 times greater than the Eddington mass corresponding to our assumed luminosity of 4.6×10^{46} ergs s^{-1}. In this paper we do not consider complications which are due to the unisotropy of some line radiation.

iii) *Models B, C, and D*

We have computed three models with different pressure laws. Their parameters were set with the following considerations. The inner radius was set such that the inner density was $\sim 10^{13}$ cm^{-3}; an outer radius was set so that the integrated intensity of [O III] λ4363 relative to Hβ did not exceed 10%. This usually corresponded to a density $\sim 10^{8.5}$ cm^{-3}. The ionization parameter was set such that at $N = 10^{10}$ cm^{-3}, $U = 10^{-2}$. This is necessary if strong C III] λ1909 is to be produced. The parameters and normalization for all models are given in Table 2, and the change of U and column density with r, in § II. The scale factor for the covering factor law was chosen so that the integration from the inner to outer radius resulted in 100% coverage of the continuum source. For comparison with actual objects, these luminosities should be multiplied by the actual covering factor of the BLR, which is thought to be in the neighborhood of 10%. The cumulative flux that is, the total luminosity in the emission lines resulting from an integration from the inner radius to a specific distance r is shown in Figures 2 and 3.

1. *Model B: constant ionization parameter.*—This model corresponds to the pressure law $N \propto r^{-2}$. Figure 2 shows cumulative flux distributions for most of the lines observed in typical AGN spectra. The models are actually characterized by a density and ionization parameter (or equivalently, flux of ionizing radiation) and are presented against radius for the specific case of an object with a luminosity in ionizing radiation of 2.5×10^{46} ergs s^{-1}. The results can be scaled to other objects by renormalizing the radial dimension by the actual luminosity in ionizing radiation, as indicated in the figure.

The upper left panel shows hydrogen and helium lines. In common with results of the following models, the line flux increases rapidly as the outer radius of the integration increases. A consequence is that the "same" formation radius of lines such as Lyα is strongly concentrated to outer radii. Most lines show a very rapid initial rise, as a result of line thermalization at the highest densities and innermost radii. He II λ4686 is less affected by thermalization than H I or He I lines because the line optical depths are generally smaller, and because of the higher charge of the ion.

Continua are compared in the upper right panel. The innermost clouds are very strong continuum sources, and the emission produced there is significant even in the net spectrum. The Lyman continuum is not plotted (for clarity) but has an intensity comparable to the others.

Carbon lines are shown in the lower left panel. The out-

TABLE 2

MODEL PARAMETERS[a]

Parameter	Model B	Model C	Model D
s	2	3/2	1
r_{min}–r_{max} (cm)	10^{17}–$10^{19.25}$	10^{17}–$10^{19.5}$	$10^{16.5}$–$10^{19.5}$
N_{max}–N_{min} (cm^{-3})	10^{13}–$10^{8.5}$	$10^{12.25}$–$10^{8.5}$	10^{12}–10^{9}
$r(N = 10^{10}$ cm$^{-3})$	$10^{18.5}$ cm	$10^{18.5}$ cm	$10^{18.5}$ cm
$U(N = 10^{10}$ cm$^{-3})$	10^{-2}	10^{-2}	10^{-2}
Column density ($N = 10^{10}$ cm^{-3})	10^{22} cm^{-2}	10^{22} cm^{-2}	$10^{22.666}$ cm^{-2}

[a] Parameters for models B, C, and D. $N \propto r^{-s}$ and $L_{ion} = 2.5 \times 10^{46}$ ergs s^{-1}. For different L_{ion}, multiply r by $(L_{ion}/2.5 \times 10^{46})^{1/2}$. The dependence of other parameters on r is given in § II.

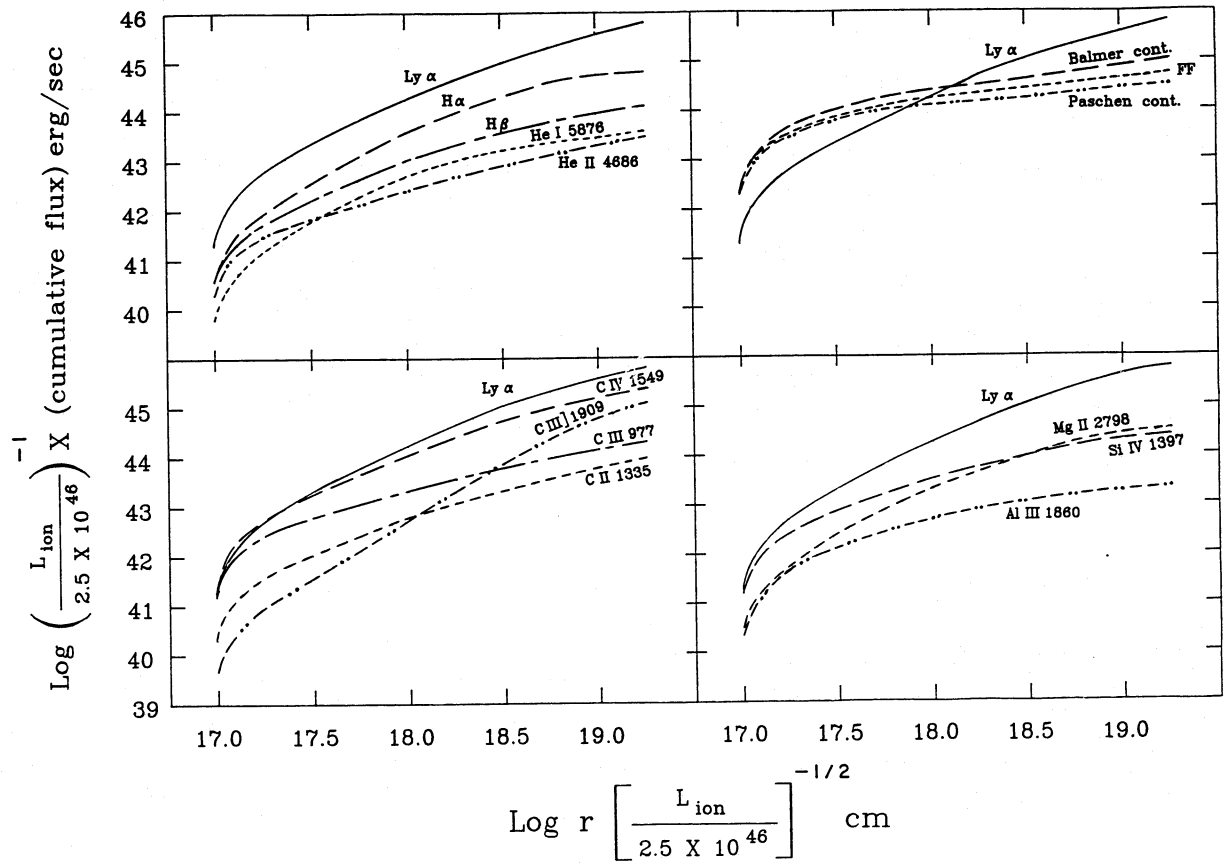

FIG. 2.—Integrated fluxes over an ensemble of clouds. Ionization parameter was set such that $U = 10^{-2}$ at $N = 10^{10}$ cm^{-3} and other parameters as listed in Table 2. Here $N \propto r^{-2}$ so that the ionization parameter is kept constant, but the cloud column density is changed, in keeping with the assumption that cloud identity is maintained. Plot shows the cumulative flux, obtained by integrating over the ensemble from the inner radius to the point indicated on the x axis. For this pressure law, most emission originates at large radius.

standing feature here is the much stronger weighting of C III] λ1909 emission to outer regions of the ensemble. This is largely due to collisional suppression of the line at densities higher than 10^{10} cm^{-3}. Other carbon lines tend to more nearly follow Lyα but are not thermalized as readily at higher densities because of their smaller optical depth. Although the details vary when the assumed pressure law changes, the tendency for the C III] λ1909 line to be formed at larger radii is a common feature of the models. This is a test of our hypothesis, since observations show that the carbon and hydrogen lines do show roughly the same profile.

Table 3 gives intensities of many of the lines predicted in this model. The table also indicates the luminosity in the line when the radial integration is stopped before 100% coverage is reached. This allows the calculations to be compared with observations in a more meaningful way. For instance, even though the majority of the emission lines are formed at larger radii for model B, some fraction of each line is formed at small radius, and will respond to rapid changes in the ionizing continuum. Model B will be consistent with the observations of many AGNs if the integration stops anywhere between the points corresponding to $r = r_{max}/2$ and $r = r_{max}$.

Figure 4 shows profiles of some of the strong lines. As expected because of the uniform ionization parameter, the profiles do not vary greatly, and are largely consistent with observations.

2. *Model C:* $N \propto r^{-3/2}$.—Here the ionization parameter decreases slowly with radius. As a result, low-ionization lines such as Mg II λ2798 are more sharply weighted to outer regions than model B, and the λ2798 line is expected to be sharper. Note again the large strength of the metal lines relative to Lyα at small radii, the enhanced Balmer continuum there, and the shallowing of the Balmer decrement as r decreases. The half-flux point (Table 3) is nearly consistent with the observed spectrum of some AGNs.

3. *Model D:* $N \propto r^{-1}$.—This law has the largest range in ionization parameter and, as a result, has the most extreme difference between high- and low-ionization lines. Integration here must stop beyond the half flux radius to be consistent with observations. As Figure 4 shows, the difference between line profiles, especially those of Lyα and the carbon lines, is probably large enough to rule out as extreme a pressure law as $N \propto r^{-1}$.

V. DISCUSSION

This study was motivated by the need to make a more realistic appraisal of the BLR environment. In particular, the BLR must have some radial extent, and the consequences of such a situation had not been considered in detail previously. We attempt to simulate actual AGN BLRs by first trying to include the microphysics occurring in dense clouds very carefully, and then using several of the many possible pressure laws to describe the density of the clouds and how this varies with radius. We do not consider all possible density laws here, but

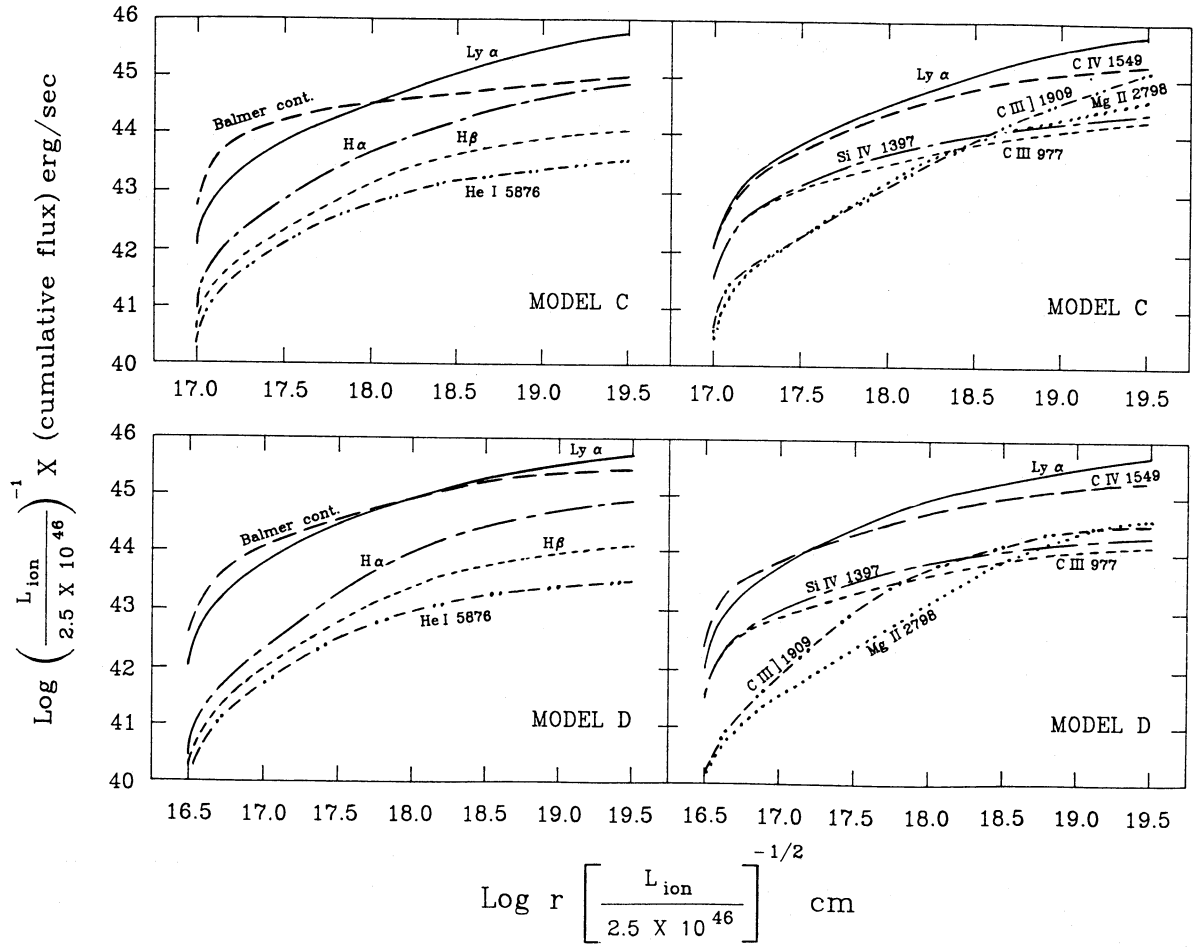

FIG. 3.—Cumulative flux for models C ($N \propto r^{-3/2}$) and D ($N \propto r^{-1}$). See Table 2 for more details.

the ones we do consider do span the range of the most likely possibilities. The densest clouds we consider are largely continuum sources and have very large optical depths. The results for such clouds are the most approximate, but we find that line emission from them has little effect on the net spectrum.

Several of the pressure laws tend to give greatest weight to outer regions of the BLR. This may help to explain the long-standing, but still surprising, result that line profile studies find similar profiles for emission lines with quite different ionization and excitation potentials, and we infer that the BLR line-emission region does not have great radial extent. This is a natural consequence of several of the more likely pressure laws. Observations of high- and low-excitation lines could be used, in combination with the type of modeling we have done here, to actually infer the pressure law within the BLR. Although the line spectrum is not sensitive to the innermost clouds, and hence there is not really a need to postulate an inner limit to the BLR, this is not true of the outer regions. The BLR must abruptly end at radii where the density falls below $\sim 10^9$ cm^{-3} if the limits to the amount of [O III] emission are not to be violated.

a) Line Ratios

Several of the calculated line ratios are those expected, but worth reemphasizing. Others are quite different from those of previous studies.

The intercombination lines are the best density indicators, as is evident from Figure 1. C III] λ1909 diminishes as N exceeds $10^{9.5}$ cm^{-3}, N III] λ1750 above $N = 10^{10}$ cm^{-3}, and the other lines (O III] λ1663, N IV λ1486, Si III] λ1893 and O IV λ1402) around $N = 10^{11}$ cm^{-3}. Some of these lines decrease only slightly, since they are thermalized only at those densities where the gas temperature is high.

The calculated intensity of Si III] λ1893 is close to that of C III] λ1909 in most models. Observational studies (e.g., Gaskell, Shields, and Wampler 1981) indicate that the contribution of

TABLE 3

PREDICTED SPECTRUM[a]

LINE	MODEL B			MODEL C			MODEL D		
	1	0.5	0.25	1	0.5	0.25	1	0.5	0.25
Lyα	53.6	29.4	21.3	54.1	30.5	23.3	44.4	35.3	37.0
Hβ	1	1	1	1	1	1	1	1	1
Hα	6.6	5.3	4.2	6.1	4.9	3.7	6.2	5.3	4.3
Pα	0.78	0.49	0.30	0.70	0.47	0.27	0.67	0.44	0.26
Ly C	5.8	6.1	9.4	5.1	5.9	9.1	9.1	15.4	27.3
Ba C	7.8	8.2	12.0	8.4	9.9	15.3	24.6	33.3	37.0
Pa C	2.9	3.5	5.5	3.3	4.5	7.5	4.7	7.9	13.7
$f-f_{cool}$	4.9	5.1	7.5	5.2	6.3	9.8	7.6	12.7	22.
He I λ5876	0.30	0.32	0.42	0.28	0.30	0.37	0.27	0.32	0.39
He II λ4686	0.26	0.18	0.19	0.23	0.21	0.25	0.18	0.22	0.30
C II λ1335	0.79	0.45	0.48	0.48	0.39	0.46	0.58	0.71	1.0
C III λ977	1.62	1.30	1.41	1.53	1.39	1.55	1.15	1.37	1.7
C III] λ1909	10.1	2.9	1.13	10.	2.9	1.35	2.9	3.3	3.9
C IV λ1549	20.6	13.7	11.5	14.6	15.1	15.0	12.8	19.3	22.4
O III] λ1663	2.90	1.67	1.13	0.41	1.83	1.57	2.17	2.50	2.93
O IV λ1402	0.55	0.33	0.28	0.43	0.45	0.54	0.69	1.25	2.1
O VI λ1035	0.01	0.01	0.02	0.05	0.09	0.18	0.87	1.78	3.4
Mg II λ2798	2.7	2.2	1.8	3.5	2.0	1.5	3.8	1.5	0.8
Si III] λ1893	3.8	2.9	2.8	4.2	2.8	2.5	3.2	2.7	2.3
Si IV λ1397	2.4	2.0	2.1	2.0	2.1	2.5	1.7	2.6	3.3
Al III λ1860	0.19	0.22	0.31	0.19	0.20	0.27	0.17	0.21	0.29
log (*N*)	8.5	9.65	10.3	8.5	9.66	10.3	9.0	9.91	10.36
log *f*(Hβ)	44.04	...	...	44.07	...	...	44.07	...	...

[a] Integrated fluxes relative to Hβ. The different columns give the result when integration stops at r_{max} (Table 2), $0.5r_{max}$, and $0.25r_{max}$.

the silicon line to the 1909 Å feature is about 20%; thus, this feature provides a good upper limit to the total contribution from very high density clouds. Note, however, that the silicon abundance is not known, and the atomic data are not as good as for carbon.

We find Si IV λ1397 to be the major contributor to the 1400 Å blend. The observational situation with regards to this has been investigated by Wills and Netzer (1979) and Gaskell, Shields, and Wampler (1981). Our results agree better with the latter and predict, in fact, a shorter mean wavelength than the one observed. The silicon abundance is, of course, very crucial here as well.

The Paschen continuum provides the best limits on the relative contribution of the high-density gas. Most AGNs do not show such a feature, and the observational limit is of the order of 3–4 times the Hβ flux. This limit is rather insensitive to uncertainties in the calculations of Hβ. For models B, C, and D, we find that the 50% $F(H\beta)$ point is about the minimum radius where we can truncate the cloud distribution and still be consistent with the observed Paschen continuum. Other continua are important too, but only at higher density; Balmer continuum is observed to be strong (Wills, Netzer, and Wills 1985), and the spectral distribution of the Lyman continuum makes it difficult to estimate its strength (see Carswell and Ferland 1988).

b) *Line Profile and Dynamics*

Gas motion and the dynamics of the BLR clouds have not been investigated in this paper. Acceleration by radiation pressure, or a wind, can give a velocity field different from the one assumed here. Thus, the radial dependence of the cloud parameters may change as well. Once this dependence is specified, the combination of line profile and intensity is a powerful tool for investigating the gas distribution. It provides an observational way to restrict the parameter space and to exclude some possibilities. The disagreement we found in model D between the predicted profiles of Lyα and C IV λ1549 is such an example.

An interesting feature of models C and D, and other models where the ionization parameter increases inward, is that the large column density clouds, close to the center, can become optically thin to the Lyman continuum. This may permit efficient acceleration by radiation pressure which then modifies the overall velocity field. In addition, we find that at such high densities free-free and H^- absorption are important, which adds yet another contribution to radiation acceleration, not affected by the onset of an ionization front in the cloud. This process has not been considered before.

c) *The Size of the BLR*

Several recent papers (e.g., Peterson *et al.* 1985; Gaskell and Sparke 1986; Clavel *et al.* 1987; see review by Peterson 1988) discuss line reverberation measurements and the comparison with the prediction of the standard model. The interpretation of the measurements is still rather uncertain because of severe undersampling and the uncertain geometry of the BLR (Maoz and Netzer 1989; Edelson and Krolik 1988).

Here we are only concerned with the estimate of the BLR size, as deduced from our calculations. For this purpose, we use models B and C, and note that the radius corresponding to the 50% Hβ flux gives a reasonable fit to the observed UV spectrum of Seyfert 1 galaxies. Thus, this is a good outer boundary for such objects. Typical line variability, during a period of large continuum fluctuations, is about factor of 2 or less, compared with the maximum line flux; i.e., the radius of interest is

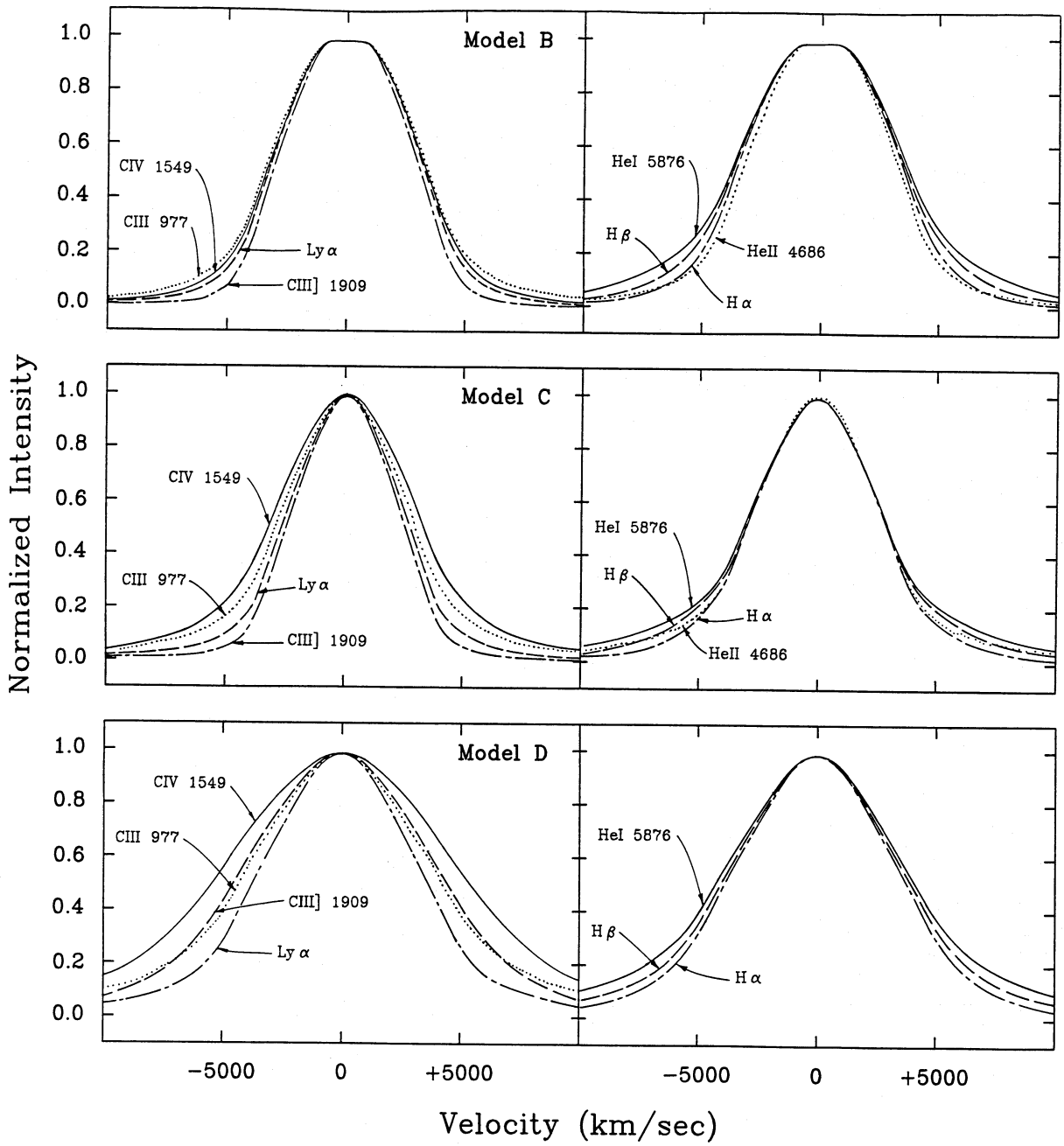

FIG. 4.—Line profiles for the various models, assuming that the cloud motion is virialized

where the cumulative line flux reaches the 50% point. For models B and C, this is the $0.25f(\mathrm{H}\beta)$ radius in Table 3. Using the dimensions thus obtained, and scaling them down to the observed luminosities as per the references below, with $H_0 = 75$ km s^{-1} Mpc^{-1}, we get the following results:

1. *NGC 4151.*—The Clavel *et al.* (1987) data suggest that the very broad C IV λ1549 component comes from a region of about 5 lt-day, and the rest of the line is 2–3 times larger. Our models give 19 lt-day.

2. *Ark 120.*—New estimates by Peterson (1989, private communication) suggest a typical dimension of 25–55 lt-day. Our models predict for this galaxy a minimal dimension of about 120 lt-day.

3. *F–9.*—Clavel, Wamsteker, and Glass (1989) give a BLR size of about 100–200 lt-day. Our models, combined with the average ultraviolet flux measurements, give 250 or more lt-day.

The new model calculations are within a factor of 2–4 of the empirically deduced BLR size. This reduces the discrepancy with the observations compared with previous, single-N theoretical estimates but does not solve the problem. Thus, we conclude that models with realistic gas distribution do have some advantage, and the small contribution of the high-N clouds means somewhat smaller BLRs in AGNs. If more and improved line reverberation studies show similar results, then new explanations are to be looked for. There are indications that this is indeed the case both from observational (Maoz *et*

al. 1989) and theoretical (Ferland and Persson 1989; Netzer 1989) works.

d) Conclusions

The models calculated in this paper represent a major improvement over previous studies of this nature by improving the treatment of many physical processes at the high-density limit and by taking into account a realistic cloud distribution. Only a small sample of all possible cases was investigated. In particular, our choice of normalization (Table 2) is arbitrary, and better agreement with the overall spectrum can be obtained for different conditions. An obvious choice would be a higher ionization parameter for the same density. Such models have been investigated by Netzer (1987) in the context of the nonisotropic radiation field of an accretion disk and by Ferland and Persson (1989). They were found to improve the agreement with the observation of the high-excitation lines and produce smaller BLRs. Different column density should be investigated also, as well as other ionizing continua.

Despite these reservations, it is possible to reach several conclusions regarding the properties of the emitting gas in the BLR. Most line emission is from densities of order 10^{9-11} cm^{-3}; the absence of several high-excitation lines and strong diffuse continua, and the presence of C III λ1909, shows this to be the case. For the pressure laws we considered, the emissivity of the ensemble of clouds is very strongly weighted to the largest radii, and the net spectrum is dominated by emission from the lowest density clouds. This offers a solution to the question of why single density model clouds ever worked as well as they did. It is very difficult to "fine tune" a radial pressure law which allows clouds of many radii to contribute to the net spectrum equally. For geometries in which a wide range of radii do contribute to the emissivity, the computed line profiles do not agree to the extent required by the observations. We are left with the most natural BLR geometry, any of several pressure laws in which the emissivity is most strongly weighted to the largest radii and lowest densities. This leaves open two questions: (*a*) Why does the BLR stop abruptly? (*b*) Why are the small radii inferred by line continuum reverberation studies still at odds with the "standard" value of the ionization parameter?

G. J. F. acknowledges the support of the National Science Foundation through grant AST 87-19607 and SERC as a Senior Visiting Fellow at the Institute of Astronomy, Cambridge. The support of the US–Israel Binational Foundation through grant 85/00085 made this collaboration possible. H. N. also thanks the OSU Astronomy Department for support.

REFERENCES

Aggarwall, K. M. 1983, *M.N.R.A.S.*, **202**, 15.
Alloin, D., Boisson, C., and Pelat, D. 1988, *Astr. Ap.*, **200**, 17.
Almog, D., and Netzer, H. 1989, *M.N.R.A.S.*, in press.
Avrett, E. H., and Loeser, R. 1988, *Ap. J.*, **331**, 211.
Bahcall, J. N., and Kozlovsky, B.-Z. 1969, *Ap. J.*, **155**, 1077.
Baldwin, J. A. 1977, *M.N.R.A.S.*, **178**, 67.
Baldwin, J. A., and Netzer, H. 1978, *Ap. J.*, **226**, 1.
Bates, D. 1962, *Proc. Roy. Soc. London A*, **267**, 297.
Berrington, K. A., and Kingston, A. E. 1987, *J. Phys. B*, **20**, 6631.
Bonilha, J., French, R., Salpeter, E., Slater, G., and Noerdlinger, P. 1979, *Ap. J.*, **233**, 649.
Brocklehurst, M. 1971, *M.N.R.A.S.*, **153**, 471.
Callaway, J. 1988, *Phys. Rev. A*, **37**, 3692.
Canfield, R. C., McClymont, A. N., and Puetter, R. C. 1984, in *Methods in Radiative Transfer*, ed. W. Kalkofen (New York: Cambridge University Press), p. 101.
Canfield, R. C., and Puetter, R. C. 1980, *Ap. J. (Letters)*, **236**, L7.
Carswell, R. F., and Ferland, G. J. 1988, *M.N.R.A.S.*, **235**, 1121.
Clavel, J., *et al.* 1987, *Ap. J.*, **321**, 251.
Clavel, J., Wamsteker, W., and Glass, I. 1989, *Ap. J.*, **337**, 236.
Collin-Souffrin, S., and Dumont, D. 1986, *Astr. Ap.*, **166**, 13.
Cota, S. 1987, Ph.D. thesis, Ohio State University.
Crenshaw, D. M. 1986, *Ap. J. Suppl.*, **62**, 821.
Davidson, K. 1972, *Ap. J.*, **171**, 213.
———. 1977, *Ap. J.*, **218**, 20.
Davidson, K., and Netzer, H. 1979, *Rev. Mod. Phys.*, **51**, 715.
Eastman, R. G., and MacAlpine, G. M. 1985, *Ap. J.*, **299**, 785.
Edelson, R. A., and Krolik, J. H. 1989, *Ap. J.*, **333**. 646.
Elitzur, M. 1984, *Ap. J.*, **280**, 653.
Elitzur, M., and Ferland, G. J. 1985, *Ap. J.*, **305**, 35.
Elitzur, M., and Netzer, H. 1984, *Ap. J.*, **291**, 464.
Fabian, A. C., Guilbert, P., Arnaud, K., Shafer, R., Tennant, A., and Ward, M. 1986, *M.N.R.A.S.*, **280**, 574.
Feldman, F. R., and MacAlpine, G. M. 1978, *Ap. J.*, **221**, 486.
Ferland, G. J., and Persson, S. E. 1989, *Ap. J.*, **347**, 656.
Ferland, G. J., Netzer, H., and Shields, G. A. 1979, *Ap. J.*, **232**, 382.
Ferland, G. J., and Rees, M. J. 1988, *Ap. J.*, **332**, 141.
Gaskell, C. M., Shields, G. A., and Wampler, E. J. 1981, *Ap. J.*, **249**, 443.
Gaskell, C. M., and Sparke, L. S. 1986, *Ap. J.*, **305**, 175.
Grandi, S. 1983, *Ap. J.*, **268**, 591.
Harrington, J. P. 1972, *Ap. J.*, **176**, 127.
Hubbard, E., and Puetter, R. C. 1984, *Ap. J.*, **290**, 394.
Hummer, D. G., and Kunasz, P. B. 1980, *Ap. J.*, **236**, 609.
Hummer, D. G., and Storey, P. 1987, *M.N.R.A.S.*, **224**, 801.
Janev, R. K., Langer, W. D., Evans, K., and Post, D. 1987, *Elementary Processes in Hydrogen-Helium Plasmas* (Berlin: Springer).
Johnson, L. C. 1972, *Ap. J.*, **174**, 227.
Kallman, T., and Kolik, J. 1986, *Ap. J.*, **308**, 805.
Kallman, T., and McCray, R. 1980, *Ap. J.*, **242**, 615.
Kallman, T., and Mushotzky, R. F. 1985, *Ap. J.*, **292**, 49.
Karzas, W. J., and Latter, R. 1961, *Ap. J. Suppl.*, **6**, 167.
Kazanas, D. 1989, *Ap. J.*, **347**, 74.
Krolik, J. 1988, *Ap. J.*, **325**, 182.
Krolik, J., and Kallman, T. 1988, *Ap. J.*, **324**, 714.
Krolik, J., and McKee, C. M. 1978, *Ap. J. Suppl.*, **37**, 459.
Krolik, J., McKee, C. M., and Tarter, C. B. 1981, *Ap. J.*, **249**, 422.
Kwan, J. 1984, *Ap. J.*, **283**, 70.
Kwan, J., and Krolik, J. H. 1981, *Ap. J.*, **250**, 478.
Lutz, W. 1967, *Ap. J. Suppl.*, **14**, 207.
MacAlpine, G. M. 1972, *Ap. J.*, **175**, 11.
———. 1981, *Ap. J.*, **251**, 465.
Maoz, D., and Netzer, H. 1989, *M.N.R.A.S.*, **236**, 21.
Maoz, D., *et al.* 1990, *Ap. J.*, in press.
Mathews, W. G., and Ferland, G. J. 1987, *Ap. J.*, **323**, 456.
Mihalas, D. 1978, *Stellar Atmospheres* (San Francisco: Freeman).
Mushotzky, R. F., and Ferland, G. J. 1984, *Ap. J.*, **278**, 558.
Netzer, H. 1978, *Ap. J.*, **219**, 822.
———. 1987, *M.N.R.A.S.*, **225**, 55.
———. 1989, *Comm. Ap.*, in press.
Netzer, H., and Davidson, K. 1979, *M.N.R.A.S.*, **187**, 871.
Netzer, H., Elitzur, M., and Ferland, G. J. 1985, *Ap. J.*, **299**, 752.
Netzer, H., and Ferland, G. J. 1984, *Pub. A.S.P.*, **96**, 593.
Osterbrock, D. E. 1988, *Astrophysics of Gaseous Nebulae and Active Galactic Nuclei* (Mill Valley, CA: University Science Books).
Penston, M. V. 1988, *M.N.R.A.S.*, **233**, 601.
Peterson, B. M. 1988, *Pub. A.S.P.*, **100**, 94.
Peterson, B. M., Meyers, K., Capriotti, E. R., Foltz, C., Wilkes, B., and Miller, H. 1985, *Ap. J.*, **292**, 164.
Puetter, R. C. 1981, *Ap. J.*, **251**, 446.
Rees, M. 1987, *M.N.R.A.S.*, **228**, 47.
Saraph, H., and Seaton, M. J. 1980, *M.N.R.A.S.*, **193**, 617.
Scoville, N., and Norman, C. 1988, *Ap. J.*, **332**, 163.
Seaton, M. J. 1978, *M.N.R.A.S.*, **185**, 5.
Shuder, J. M. 1982, *Ap. J.*, **259**, 48.
Shull, J. M., and Van Steenburg, M. E. 1985, *Ap. J.*, **298**, 268.
Smith, M. G., *et al.* 1981, *M.N.R.A.S.*, **195**, 437.
Vriens, L. and Smeets, A. H. M. 1980, *Phys. Rev. A*, **22**, 940.
Weisheit, J. C., Shields, G. A., and Tarter, C. B. 1981, *Ap. J.*, **324**, 717.

Weymann, R. J., and Williams, R. E. 1969, *Ap. J.*, **157**, 1201.
Wilkes, B., and Elvis, M. 1987, *Ap. J.*, **323**, 243.
Wilkes, B. J., and Carswell, R. F. 1982, *M.N.R.A.S.*, **201**, 645.
Wills, B. J.,Netzer, H., and Wills, D. 1985, *Ap. J.*, **288**, 94.
Wills, D., and Netzer, H. 1979, *Ap. J.*, **233**, 1.
Zheng, W. 1989, *Ap. J.*, **337**, 617.

G. F. FERLAND: Department of Astronomy, Ohio State University, 174 West 18th Avenue, Columbus, OH 43210-1106

HAGAI NETZER: School of Physics and Astronomy, Tel Aviv University, Ramat Aviv, Tel Aviv 69978, Israel

M. J. REES: Institute of Astronomy, Cambridge University, Madingley Road, Cambridge, CB3 0HA, England, UK